Rev. Roum. Sci. Techn.– Électrotechn. et Énerg.
Vol. **70**, *2*, pp. 253–258, Bucarest, 2025

NOVEL ACCURATE NANOSATELLITE ATTITUDE ESTIMATION AND CONTROL ARCHITECTURE BASED ON MAGNETIC DIPOLE MOMENT AND ACTUATOR FAULT COMPENSATION

ROUBACHE RIMA[1], ADNANE AKRAM[1], BEKHADDA NACERA[1], BENMANSOUR JALAL EDDINE[1]

Keywords: Nanosatellite; Varying residual magnetic moment (RMM) compensation; Extended Kalman filter (EKF); Particle swarm optimization (PSO); Actuator faults; Adaptive proportional derivative (APD).

Nanosatellites are increasingly considered an effective alternative to traditional solutions for Earth observation missions from space. The attitude determination and control system (ADCS) is one of the key subsystems of a nanosatellite, critical for the mission's success. This paper investigates the design of an extended Kalman filter (EKF) for a nanosatellite attitude determination along with the residual magnetic moment and the actuator fault compensation. The proposed architecture relies on a heuristic extended Kalman filter (HEKF) and adaptive proportional-derivative (APD) controller. The optimized filtering system searches for the best measurement covariance and process noise matrices to track the best estimation of the attitude and residual magnetic moment disturbance. Additionally, the APD controller, based on an observer, is designed to cope with uncertainties in actuator failure and provide reliable attitude control for the nanosatellite. The investigated attitude filtering and control scheme is examined through numerical simulation to determine whether it offers benefits in terms of performance and convergence behavior.

1. INTRODUCTION

Recently, nanosatellites have carved out their specialized role in advanced missions because of their small size, reduced practical cost, and short development period [1]. It is a common requirement in these advanced missions to meet strict attitude requirements to obtain scientific data and/or high-resolution Earth images [2,3]. To fulfill these missions, one of the key functions is the attitude determination and control system (ADCS). Whereas, the main encountered challenges are achieving higher ADCS accuracy with a minimal number of sensors and actuators [4].

One of the most significant constraints for the design of the ADCS is the external disturbance torques. In low Earth orbit nanosatellites, the magnetic dipole moment, referred to as the residual magnetic moment, represents the foremost attitude disturbance, which leads to an unfavorable effect on the attitude control accuracy [5]. The onboard electric current loop, a small permanent magnet in some devices, or some special material on the satellite mainly causes the magnetic disturbance. It does not strongly depend on the satellite [6,7]. This disturbance may be compensated on the ground by a good engineering practice [8,9] or in-orbit with an active control strategy [6,10]. The on-ground residual magnetic moment (RMM) mitigation method is based on a so-called magnetic cleanliness program, which involves reducing the magnetic sources on each part or subsystem of the satellite [9]. Although the magnetic disturbances of the nanosatellite are considerably mitigated by the application of the on-ground magnetic cleanliness technique, these disturbances cannot be entirely rejected. Therefore, it is paramount to apply in-orbit residual magnetic moment compensation based on filtering methods to get a precise attitude for the nanosatellite.

The first in orbit RMM compensation method was applied to the SNAP1 nanosatellite by using a Kalman filter to estimate the magnetic dipole moment, where the estimator output is partially compensated by magnetorquers [11]. In [12], the authors proposed two methods for paying the RMM using an extended Kalman filter (EKF) and an unscented Kalman filter (UKF) for accurate attitude estimation, respectively. Söken et al. proposed a method to compensate for the time-variable magnetic moment, both in-orbit and in the design phase of the satellites [6,7]. Recently, Söken proposed an attitude filtering and magnetometer calibration approach for nanosatellites, utilizing magnetometers, sun sensors, and gyros [13]. The satellite attitude and bias terms for the gyros and magnetometers are estimated through a combined TRIAD-UKF method. Earlier, the performance of the attitude motion determination algorithm for the SiriusSat-1 (space weather research nanosatellite) was presented in [14], where an EKF was applied based on the magnetometer only to track the magnetometer bias in real-time. Attitude estimation problems for nanosatellites using microsensors based on decentralized information fusion are investigated using MEMS gyroscopes, magnetometers, and miniature sun sensors [15].

On the other hand, various approaches to nanosatellite attitude control have been widely explored in the literature, including linear quadratic regulators and proportional derivative (PD) controllers [16, 17], among others. In [16], a linear quadratic controller is used for Virginia Tech HokieSat to stabilize the orientation of the nanosatellite with magnetic control. Furthermore, the conventional PD controller was stated as an adequate way to preserve the desired attitude performance and has been effectively implemented due to its fast transient response as well as its accurate steady-state error [18]. Specially, PD control law was adopted to adjust the Tian Tuo 1 nanosatellite to the desired orientation [17].

From the works above, it can be observed that there are still some challenging issues to be addressed in the design of the ADCS. First, it is worth noting that some presented methods are developed based on both a magnetometer and a sun sensor. The main drawback in the design of these methods is the unavailability of the sun sensor data in the satellite's eclipse phase, which leads to the degradation of the estimation results. Additionally, the use of multiple sensors on board the nanosatellite is inappropriate due to the restrictions on size, cost, and power consumption. To weed out these constraints, the estimation using only the magnetometer should receive more attention, as this sensor is characterized by its lightweight, reliability, and low power consumption. Furthermore, it is desirable to take into consideration the magnetic moment disturbance changes, which is more practical [7]. Unfortunately, this is usually neglected in most existing works [11]. Additionally, it is

[1] Department of Research in Space Mechanics, Satellite Development Center, Algerian Space Agency, BP 4065, Ibn Rochd Usto, 31130, Oran, Algeria. E-mails: rroubache@cds.asal.dz (correspondence), aadnane@cds.asal.dz, nbekhadda@cds.asal.dz, jebenmansour@cds.asal.dz

DOI: 10.59277/RRST-EE.2025.2.17

observed in some aforementioned works that the design of an effective operational Kalman filter depends largely on the knowledge accuracy of process covariance and measurement noise covariance matrices. Wherein, an improper tuning of these matrices may cause undesired performance and it can even induce practical divergence. On the other side, the above-mentioned controllers [16,17] gave satisfactory results, but they have been adopted under the basic hypothesis that the actuator faults are not taken in consideration. Whereas, the unknown actuator uncertainties are frequently encountered in practical applications due to harsh space environments, manufacturing imperfections and wearing out of the mechanical and electrical components of actuators [19]. These faults may cause significant degradation of the nominal controller's performance or even lead to the instability. Hence, it is necessary to handle the loss-of-effectiveness actuator faults in the attitude controller design intending to guarantee the desired performance for the nanosatellite.

Inspired by the previously mentioned woks, this current paper addresses the problem of the nanosatellite attitude estimation and control under the effect of time varying RMM and unknown actuator uncertainties. A heuristic algorithm based on a particle swarm optimization is proposed to find the optimal process and measurement noise covariance matrices for the EKF. Moreover, an adaptive proportional derivative controller is designed in order to cope with the actuator uncertainties and keep a stable and an accurate attitude control of the nanosatellite. The proposed architecture is able to counteract the impact of those sudden changes in effective manner.

The reminder of this paper is organized as follows: nanosatellite model dynamic and problem formulation are provided in section 2. Heuristic filtering design is given in section 3. The ADCS design under actuator uncertainty is presented in section 4. Numerical simulations are given in section 5. Finally, conclusion is drawn in section 6.

2. PRELIMINARIES AND PROBLEM STATEMENT

This section describes the attitude dynamics equation of the nanosatellite and magnetometer sensor model [10, 20, 21].

2.1 NANOSATELLITE DYNAMIC MODELLING

A model of the Nanosatellite's attitude dynamics used along this study is expressed as follows [21]

$$\mathbf{I}\dot{\omega} = -\omega \times (\mathbf{I}\omega + \mathbf{h}) + \mathbf{u} + \mathbf{T}_d + \mathbf{u}_f, \quad (1)$$

with

$$\mathbf{T}_d = \mathbf{M} \times \mathbf{B}. \quad (2)$$

where ω is the inertially referenced body angular rate, I is the satellite inertia, $\mathbf{h}$ is the reaction wheel's angular momentum, u is the reaction wheel control torque, B is the earth magnetic field, $\mathbf{M}$ is the residual magnetic moment of the satellite and $\boldsymbol{u}_f$ denotes the actual actuator fault.

In this study, we consider a scenario where the RMM terms are modeled as constant but with unexpected abrupt changes. The dynamic of the RMM is given by the following equation:

$$\dot{M}_j = 0. \quad (3)$$

with the supposition that

$$M_j(t) = \begin{cases} M_0, & t_0 \le t < t_1 \\ M_1, & t_1 \le t < t_2 \\ \vdots & \vdots \\ M_n, & t_n \le t < t_{orb} \end{cases} \quad (4)$$

Here t_j are the unknown time instances that a change occurs within one orbit period t_{orb}, M_j are constant RMM vectors for $j = 1, \dots n$.

Considering the unit quaternion vector defined as $\mathbf{q} = [q_1,\ q_2,\ q_3,\ q_4]^T = [\boldsymbol{q}_v,\ q_4]^T$.
The nanosatellite kinematic differential equation in terms of quaternion can be expressed as [19, 20]

$$\dot{\mathbf{q}} = \begin{bmatrix} \dot{\boldsymbol{q}}_v \\ \dot{q}_4 \end{bmatrix} = \frac{1}{2}\boldsymbol{\Lambda}(\boldsymbol{q}_v, q_4)\omega. \quad (5)$$

with

$$\boldsymbol{\Lambda}(\boldsymbol{q}_v, q_4) = \begin{bmatrix} q_4\boldsymbol{I}_{3\times3} + [\boldsymbol{q}_v{}^{\times}] \\ -\boldsymbol{q}_v \end{bmatrix}. \quad (6)$$

Here $[\boldsymbol{q}_v{}^{\times}] \in R^{3\times3}$ is a skew symmetric matrix

$$[\mathbf{q}_v{}^{\times}] = \begin{bmatrix} 0 & -q_3 & q_2 \\ q_3 & 0 & -q_1 \\ -q_2 & q_1 & 0 \end{bmatrix}. \quad (7)$$

The unit quaternion is also subject to the following quadratic constraint equation

$$q_4^2 + \mathbf{q}_v^{\mathrm{T}}\boldsymbol{q}_v = 1. \quad (8)$$

2.2 MAGNETOMETER SENSOR MODEL

The measurements model of the magnetometer sensor can be expressed as [20, 22]

$$\widetilde{\boldsymbol{B}} = \mathbf{A}(\boldsymbol{q})\boldsymbol{B}^{\mathrm{o}} + \boldsymbol{\eta}_1. \quad (9)$$

where $\boldsymbol{\eta}_1$ is a vector of Gaussian white noise with zero mean and covariance matrix $\boldsymbol{\delta}_1^2$, $\boldsymbol{B}^o$ is the geomagnetic field vector expressed in the orbital coordinate frame, $\widetilde{\boldsymbol{B}}$ is the actual measurement value of the magnetometer and $\mathbf{A}(\boldsymbol{q})$ is attitude transformation matrix, which is calculated as [10]

$$\mathbf{A}(\boldsymbol{q}) = (q_4^2 - \boldsymbol{q}_v{}^T\boldsymbol{q}_v)\boldsymbol{I}_{3\times3} + 2\boldsymbol{q}_v{}^T\boldsymbol{q}_v - 2q_4[\boldsymbol{q}_v{}^{\times}]. \quad (10)$$

ASSUMPTION 1. *The magnetometer is assumed to be calibrated on-ground before the flight through a calibration approach.*

2.3 RESEARCH PROBLEM STATEMENT

To addresses the problem of the estimation and control of nanosatellite attitude in presence of time varying RMM and unknown actuator faults, the following tasks are investigated: **Task 1.** Determining the required time-varying RMM necessary to achieve accurate attitude estimation for a nanosatellite. **Task 2.** Enhancing the performance of the EKF by optimizing its parameters through Particle Swarm Optimization to achieve more accurate attitude estimation. **Task 3.** Compensating unexpected faults in actuators to maintain the desired attitude control performance. Figure 1 presents the overall block diagram of the attitude filtering and control architecture for nanosatellite. A HEKF is adopted based on particle swarm optimization (PSO) algorithm for an accurate attitude estimation ($\boldsymbol{q}_v$ and $\boldsymbol{\omega}$), in such away the RMM $\widehat{\mathbf{M}}$ is constantly compensated. Besides, an APD controller is considered for the purpose of controlling the

nanosatellite attitude and eliminating the actuator torque fault influences $\boldsymbol{u}_f$.

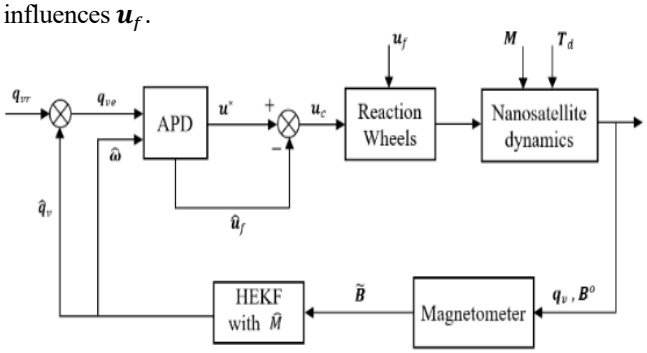

Fig. 1 – Overall block diagram of attitude filtering and control architecture.

3. ATTITUDE FILTERING DESIGN IN THE PRESENCE OF RMM EFFECT

3.1 CONVENTIONAL EKF

In this subsection, a conventional EKF algorithm is applied for nanosatellite attitude and RMM estimation (**Task 1**). The suggested filter is capable of estimating and isolating any unexpected RMM in real time, resulting in accurate attitude assessment. An algorithm description of the EKF is described in such a way that the state vector to be estimated is ten dimensional composed of quaternions, body angular rates and RMM terms, are specified by

$$\boldsymbol{X} = [\boldsymbol{q} \quad \boldsymbol{\omega} \quad \boldsymbol{M}]^{\mathrm{T}} \tag{11}$$

The EKF algorithm consists of two steps: propagation and correction cycles, as shown below [23].

Step (1): Propagation cycle

The satellite dynamics states are propagated by numerical integration using the following equations

$$\overline{\boldsymbol{q}}_k = \widehat{\boldsymbol{q}}_k + \frac{1}{2}\int_{t_k}^{t_{k+1}} \boldsymbol{\Lambda}(\widehat{\boldsymbol{\omega}}_k)\,\widehat{\boldsymbol{q}}_k \mathrm{d}t. \tag{12}$$

and

$$\overline{\boldsymbol{\omega}}_k = \widehat{\boldsymbol{\omega}}_k + \int_{t_k}^{t_{k+1}} \left[\boldsymbol{I}^{-1}(-\widehat{\boldsymbol{\omega}}_k \times (\boldsymbol{I}\widehat{\boldsymbol{\omega}}_k + \boldsymbol{h}) + \boldsymbol{u} - \widehat{\boldsymbol{M}}_k \times \boldsymbol{B})\right]\mathrm{d}t. \tag{13}$$

and

$$\overline{\boldsymbol{M}}_k = \widehat{\boldsymbol{M}}_k + \int_{t_k}^{t_{k+1}} -\frac{1}{\tau}\widehat{\boldsymbol{M}}_k \mathrm{d}t\,. \tag{14}$$

then

$$\overline{\boldsymbol{X}}_k = [\overline{\boldsymbol{q}}_k \quad \overline{\boldsymbol{\omega}}_k \quad \overline{\boldsymbol{M}}_k]^{\mathrm{T}}. \tag{15}$$

The state transition matrix is given by

$$\boldsymbol{\Phi}_k \approx \boldsymbol{I}_{10\times 10} + \begin{bmatrix} \left.\frac{\partial \dot{\boldsymbol{q}}}{\partial \boldsymbol{q}}\right|_{t=t_k} & \left.\frac{\partial \dot{\boldsymbol{q}}}{\partial \omega}\right|_{t=t_k} & \left.\frac{\partial \dot{\boldsymbol{q}}}{\partial \boldsymbol{M}}\right|_{t=t_k} \\ \left.\frac{\partial \dot{\boldsymbol{\omega}}}{\partial \boldsymbol{q}}\right|_{t=t_k} & \left.\frac{\partial \dot{\boldsymbol{\omega}}}{\partial \boldsymbol{\omega}}\right|_{t=t_k} & \left.\frac{\partial \dot{\boldsymbol{\omega}}}{\partial \boldsymbol{M}}\right|_{t=t_k} \\ \left.\frac{\partial \dot{\boldsymbol{M}}}{\partial \boldsymbol{q}}\right|_{t=t_k} & \left.\frac{\partial \dot{\boldsymbol{M}}}{\partial \omega}\right|_{t=t_k} & \left.\frac{\partial \dot{\boldsymbol{M}}}{\partial \boldsymbol{M}}\right|_{t=t_k} \end{bmatrix} T_s. \tag{16}$$

The predicted error covariance matrix is expressed as

$$\overline{\boldsymbol{P}} = \boldsymbol{\Phi}_k \widehat{\mathbf{P}}_{\mathrm{k}} \boldsymbol{\Phi}_{\mathrm{k}}^{\mathrm{T}} + \boldsymbol{Q}_k. \tag{17}$$

and $\boldsymbol{Q}_k$ is the process covariance matrix which is defined as

$$\boldsymbol{Q}_k = \mathrm{diag}\left(\boldsymbol{Q}_{q_{1,2,3,4}}, \boldsymbol{Q}_{\omega_{1,2,3}}, \boldsymbol{Q}_{M_{x,y,z}}\right). \tag{18}$$

where $T_s = t_{k+1} - t_k$ is the sampling period and $\boldsymbol{I}_{10\times 10}$ is the *10×10* dimension identity matrix.

Step-2: Correction cycle

The observation matrix is calculated as follows

$$\mathbf{H}_k = \left[\frac{\partial \widetilde{\boldsymbol{B}}}{\partial \boldsymbol{q}} \quad \frac{\partial \widetilde{\boldsymbol{B}}}{\partial \omega} \quad \frac{\partial \widetilde{\boldsymbol{B}}}{\partial \boldsymbol{M}}\right]. \tag{19}$$

where $\bar{\boldsymbol{e}}_k$ is the residual term given by

$$\bar{\boldsymbol{e}}_k = \left[\widetilde{\boldsymbol{B}}_k - \widehat{\boldsymbol{B}}_k\right]. \tag{20}$$

with $\widehat{\boldsymbol{B}} = \boldsymbol{A}(\widehat{\boldsymbol{q}})\boldsymbol{B}^o$ is the estimated value of magnetometer.

The corresponding Kalman gain is computed by the following equation

$$\boldsymbol{K}_k = \overline{\boldsymbol{P}}_k \boldsymbol{H}_k^{\mathrm{T}}\left(\boldsymbol{H}_k \overline{\boldsymbol{P}}_k \boldsymbol{H}_k^{\mathrm{T}} + \boldsymbol{R}\right)^{-1}. \tag{21}$$

where $\boldsymbol{R}$ is the measurement noise covariance matrix of magnetometer sensor. The covariance correction matrix is obtained by

$$\widehat{\boldsymbol{P}}_k = (\boldsymbol{I}_{10\times 10} - \boldsymbol{K}_k \boldsymbol{H}_k)\overline{\boldsymbol{P}}_k. \tag{22}$$

where $\widehat{\boldsymbol{P}}_k$ is the corrected error covariance matrix.

The update of the corrected state can be calculated by the following equation:

$$\widehat{\boldsymbol{X}}_k = [\widehat{\boldsymbol{q}}_k \quad \widehat{\boldsymbol{\omega}}_k \quad \widehat{\boldsymbol{M}}_k]^{\mathrm{T}} = \overline{\boldsymbol{X}}_k + \boldsymbol{K}_k \bar{\boldsymbol{e}}_k. \tag{23}$$

3.2 HEURISTIC ALGORITHM INTEGRATION

PSO algorithm is a population-based search optimization method developed in 1995 [24–26]. In this work, a heuristic filtering strategy based on PSO is proposed to find the optimal $\boldsymbol{Q}$ and $\boldsymbol{R}$ matrices for the EKF. The procedure to dealing with the optimization problem described in (**Task 2**) can be outlined as follows

- **Objective Function**: Minimize a cost function, denoted as J, which represents the quality of the EKF in terms of its ability to estimate the state variables of a dynamic system. This cost function to be minimized for the HEKF can be defined as

$$J = \sum_{t_1}^{t_f}\sum_{i}^{4} (Eq_i)^2. \tag{24}$$

where Eq_i is the ith attitude quaternion error, t_1 is the attitude stabilization time, t_f is the end of simulation.

- **Decision Variables** $\boldsymbol{Q}$ and $\boldsymbol{R}$: The elements of **Q** and **R** need to be optimized and should satisfy certain constraints to ensure that they are positive definite covariance matrices and within a feasible range.

Therefore, the optimization problem can be summarized as finding the optimal values of **Q** and **R** using PSO to minimize the cost function $\boldsymbol{J}$, ultimately leading to an EKF with improved performance in estimating the state variables of the nanosatellite dynamic system.

The integration of the PSO algorithm into the conventional estimator leads to the creation of the HEKF by adhering the following steps

Step 1: Initialization of PSO parameters
Step 2: Selection of the $\boldsymbol{Q}$, $\boldsymbol{R}$ ranges of the PSO

Step 3: Initialization of $\boldsymbol{Q}$, $\boldsymbol{R}$ values of the PSO
Step 4: Initialization of estimation error
Step 5: # Optimized EKF #
  While (Estimation error > Referential error)
    # EKF algorithm #
    While (Time < t_f)
      Initialization $\boldsymbol{x}_0, \boldsymbol{P}_0, \boldsymbol{T}_s$
      if Time == 0
        Input: $\bar{\boldsymbol{x}}_k = \boldsymbol{x}_0, \bar{\boldsymbol{P}}_k = \boldsymbol{P}_0$
      Else
        Input: $\bar{\boldsymbol{x}}_k = \hat{\boldsymbol{x}}_k, \bar{\boldsymbol{P}}_k = \hat{\boldsymbol{P}}_k$
      End
      RMM suppression eq. (11)
      State prediction: eq. (13)
      Input: $\boldsymbol{Q}$, $\boldsymbol{R}$ updated
      Error covariance prediction: eq. (14)
      Kalman gain: eq. (19)
      Update covariance error: eq. (20)
      Update state: eq. (21)
    End
    # End EKF Algorithm #
    Calculation of estimation error
    Execution of PSO algorithm
    $\boldsymbol{Q}$, $\boldsymbol{R}$ update values
  End
End optimized EKF
Step 6: $\boldsymbol{Q}$, $\boldsymbol{R}$ optimal values.

4. ATTITUDE CONTROL DESIGN UNDER ACTUATOR UNCERTAINTY

The main motivation of employing adaptive attitude control is to address such uncertainties in system parameters achieving accurate control. In this study, the RMM couple acting on the satellite attitude, as modelled in eq. (1), has been estimated and introduced into the real-time dynamics of the HEKF filter. This allows for the resulting dynamics of the system to be rewritten in an updated form eq. (25), ensuring that the control system can achieve the desired level of accuracy even in the presence of actuator uncertainties.

Therefore, the resulting dynamics of the system eq. (1) can be rewritten as follows,

$$\boldsymbol{I}\dot{\boldsymbol{\omega}} = -\boldsymbol{\omega} \times (\mathbf{I}\boldsymbol{\omega} + \mathbf{h}) + \mathbf{u} + \mathbf{u}_f. \tag{25}$$

where $\boldsymbol{u}_f$ is the unknown actuator fault.

Accordingly, an adaptive proportional derivative (APD) control law is proposed to eliminate any unexpected actuator fault during the satellite attitude tracking as follows (**Task 3**). Specifically, our control strategy leverages on eq. (25) to identify and compensate for any actuator faults in real-time, resulting in improved performance and reliability.

$$\boldsymbol{the\ u} = \omega \times (\mathbf{I}\omega + \mathbf{h}) - \mathbf{K}\boldsymbol{q}_{ve} - \mathbf{D}\omega - \hat{\boldsymbol{u}}_f. \tag{26}$$

with

$$\hat{\boldsymbol{u}}_f = \int \boldsymbol{C}(\boldsymbol{K}^{-1})^{\mathrm{T}}\omega \, \mathrm{d}t. \tag{27}$$

where $\boldsymbol{C} = \mathrm{diag}[c_1 \quad c_2 \quad c_3]$, with $c_i > 0, i = 1,2,3$ and $\boldsymbol{D}$ and $\boldsymbol{K}$ are positive gains.

ASSUMPTION 2. *Given that $\boldsymbol{u}_f$ is bounded and slow-varying, thus it is reasonable to assume that $\dot{\boldsymbol{u}}_f \approx 0$.*

THEOREM 1.

Consider the nonlinear uncertain system eq. (5) and eq. (25) in the presence of unknown actuator fault under Assumption 2. If the adaptive control law eq. (26) is implemented with actuation faults updated by eq. (27), then the trajectories of the system asymptotically converge to the equilibrium point.

Proof.

Considering the following positive Lyapunov function

$$V = \frac{1}{2}\boldsymbol{\omega}^{\mathrm{T}}\boldsymbol{K}^{-1}\boldsymbol{I}\boldsymbol{\omega} + \boldsymbol{q}_{ve}^2 + (q_{4e} - 1)^2 + \frac{1}{2}\boldsymbol{C}^{-1}\boldsymbol{e}^T\boldsymbol{e}. \tag{28}$$

From eq (8), we can obtain

$$V = \frac{1}{2}\boldsymbol{\omega}^{\mathrm{T}}\boldsymbol{K}^{-1}\boldsymbol{I}\boldsymbol{\omega} + 2(1 - q_{4e}) + \frac{1}{2}\boldsymbol{C}^{-1}\boldsymbol{e}^{\mathrm{T}}\boldsymbol{e}. \tag{29}$$

The time derivative of V can be expressed as

$$\dot{V} = \boldsymbol{\omega}^{\mathrm{T}}\boldsymbol{K}^{-1}\boldsymbol{I}\dot{\boldsymbol{\omega}} - 2\dot{q}_{4e} + \boldsymbol{C}^{-1}\boldsymbol{e}^{\mathrm{T}}\dot{\boldsymbol{e}}. \tag{30}$$

where $\boldsymbol{e} = \boldsymbol{u}_f - \hat{\boldsymbol{u}}_f$ is the default estimation error, thus $\dot{V}$ is given by

$$\dot{V} = \boldsymbol{\omega}^{\mathrm{T}}\boldsymbol{K}^{-1}\big[-\boldsymbol{\omega} \times (\boldsymbol{I}\boldsymbol{\omega} + \boldsymbol{h}) + \boldsymbol{u} + \boldsymbol{u}_f\big] - 2\dot{q}_{4e} + \boldsymbol{C}^{-1}\boldsymbol{e}^T\dot{\boldsymbol{e}}. \tag{31}$$

Substituting eq. (26) in eq. (31) yields

$$\begin{aligned}\dot{V} &= \boldsymbol{\omega}^{\mathrm{T}}\boldsymbol{K}^{-1}[-\boldsymbol{K}\boldsymbol{q}_{ve} - \boldsymbol{D}\boldsymbol{\omega} - \boldsymbol{e}] + \boldsymbol{q}_{ve}^{\mathrm{T}}\boldsymbol{\omega} + \boldsymbol{C}^{-1}\dot{\boldsymbol{e}}^{\mathrm{T}}\boldsymbol{e} \\ &= -\boldsymbol{\omega}^{\mathrm{T}}\boldsymbol{q}_{ve} - \boldsymbol{\omega}^{\mathrm{T}}\boldsymbol{K}^{-1}\boldsymbol{D}\boldsymbol{\omega} + \boldsymbol{\omega}^{\mathrm{T}}\boldsymbol{K}^{-1}\boldsymbol{e} + \boldsymbol{q}_{ve}^{\mathrm{T}}\boldsymbol{\omega} + \boldsymbol{C}^{-1}\dot{\boldsymbol{e}}^{\mathrm{T}}\boldsymbol{e} \\ &= -\boldsymbol{\omega}^{\mathrm{T}}\boldsymbol{K}^{-1}\boldsymbol{D}\boldsymbol{\omega} + (\boldsymbol{\omega}^{\mathrm{T}}\boldsymbol{K}^{-1} + \boldsymbol{C}^{-1}\dot{\boldsymbol{e}}^{\mathrm{T}})\boldsymbol{e}.\end{aligned} \tag{32}$$

According to assumption 2

$$\dot{V} = -\boldsymbol{\omega}^{\mathrm{T}}\boldsymbol{K}^{-1}\boldsymbol{D}\boldsymbol{\omega} + \big(\boldsymbol{\omega}^{\mathrm{T}}\boldsymbol{K}^{-1} - \boldsymbol{C}^{-1}\,\dot{\hat{\boldsymbol{u}}}_f^{\mathrm{T}}\big)\boldsymbol{e}. \tag{33}$$

since

$$\dot{\hat{\boldsymbol{u}}}_f = \boldsymbol{C}(\boldsymbol{K}^{-1})^T\boldsymbol{\omega}. \tag{34}$$

Hence, eq. (33) leads to

$$\dot{V} = -\boldsymbol{\omega}^{\mathrm{T}}\boldsymbol{K}^{-1}\boldsymbol{D}\boldsymbol{\omega} < 0. \tag{35}$$

Therefore, the semi-negative definiteness of $\dot{V}$ has demonstrated the asymptotic stability of the system. This completes the proof of the THEOREM 1.

5. NUMERICAL SIMULATION

This simulation is done to test the HEKF performance in the presence of unexpected abrupt changes in RMM. The estimation accuracy is investigated for a nanosatellite and then the effects of the filter tuning on the estimation accuracy and filter's tracking capability is discussed. The simulation is performed for $t_f = 30{,}000$ s. The nanosatellite inertia is selected as $\boldsymbol{I} = \mathrm{diag}(1.2,1.2,1.2)$ Kgm^2. The magnetometer sensor noise is characterized by zero mean Gaussian white noise with a standard deviation of 0.01 μT. Whereas, we assume the instantaneous change of the RMM terms is realized at the 12000th sec as shown in eq. (36).

$$\begin{cases}\boldsymbol{M} = [0.08 \;\; 0.03 - 0.05]^{\mathrm{T}}\mathrm{AM}^2 & 0 \le t < 12000\ \mathrm{s} \\ \boldsymbol{M} = [0.11 \;\; 0.02 - 0.03]^{\mathrm{T}}\mathrm{AM}^2 & 0 \le t < 30000\ \mathrm{s}\end{cases}. \tag{36}$$

The applied actuator fault is assumed to be constant, such that $\boldsymbol{u}_f = [3 \cdot 10^{-4} \quad 2 \cdot 10^{-4} \quad -2 \cdot 10^{-4}]^{\mathrm{T}}$Nm.

Table 1 provides the PSO algorithm's parameters.

Table 1
PSO parameters

Parameters	*Value*
Number of particles	20
Number of iterations	10
Inertia Weight (w)	0.7298
Acceleration constant (c_1=c_2)	1.4961

$\boldsymbol{Q}$ and $\boldsymbol{R}$ ranges	$10^{-11} \cdot \boldsymbol{I}_4 \leq \mathbf{Q}_q \leq 10^{-7} \cdot \boldsymbol{I_4}$ $10^{-17} \cdot \boldsymbol{I}_4 \leq \mathbf{Q}_\omega \leq 10^{-13} \cdot \boldsymbol{I}_4$ $10^{-10} \cdot \boldsymbol{I}_4 \leq \mathbf{Q}_M \leq 10^{-6} \cdot \boldsymbol{I}_4$ $0.1 \cdot \boldsymbol{I}_3 \leq \mathbf{R} \leq 0.5 \cdot \boldsymbol{I}_3$

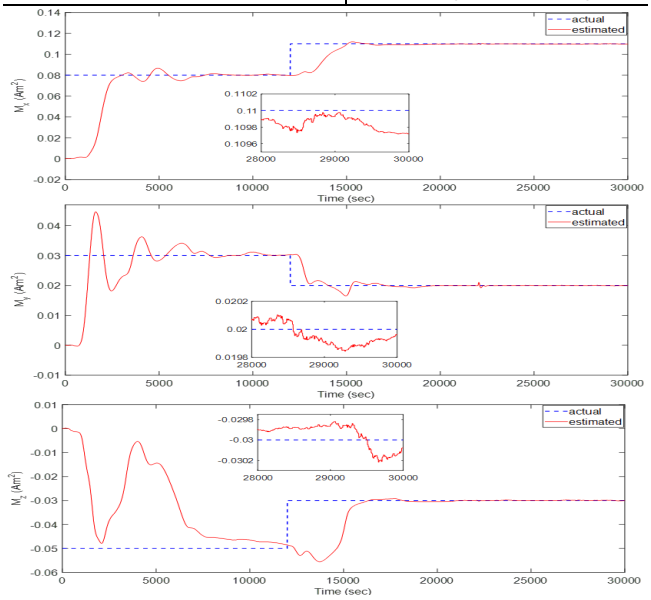

Fig. 2 – Estimation of the RMM in case of a sudden change.

After the execution of PSO algorithm for RMM and attitude filtering, the obtained optimal measurement covariance and process noise matrices are given in Table 2. Note that the considered errors for the fitness function evaluation of the PSO are calculated after $t_1 = 28000$ s.

Table 2

Optimal HEKF parameters

Parameters	*Value*
The optimal $\boldsymbol{Q}_q$	$2.6025 \cdot 10^{-10} \cdot \boldsymbol{I}_4$
The optimal $\boldsymbol{Q}_\omega$	$9 \cdot 9949.10^{-14} \cdot \boldsymbol{I}_4$
The optimal $\boldsymbol{Q}_M$	$1.0490 \cdot 10^{-8} \cdot \boldsymbol{I}_4$
The optimal $\boldsymbol{R}$	$0.3848 \cdot \boldsymbol{I}_3$

The estimation results of the time varying RMM are shown in Fig. 2. It is clearly seen that at t =12000 s there is a sudden change in the level of disturbance. The proposed filter based on PSO tracks accurately and agilely catch the new value of the actual magnetic moment disturbance. The estimation performance of the filter mainly depends on the output of the PSO optimizer ($\boldsymbol{Q}$ and $\boldsymbol{R}$ matrices).

Figure 3 illustrates the residual magnetic moment estimation errors by using HEKF estimator. The results demonstrate a good online RMM estimation both before and after the sudden change of the actual magnetic dipole moment (The estimation errors are around $2 \cdot 10^{-4}$Am^2).

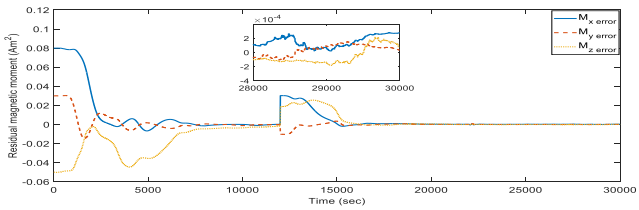

Fig. 3 – Residual magnetic moment estimation errors.

A deterministic error metric based on root mean squared error (RMSE) is evaluated for the RMM and attitude terms between the 28000th and 30000th seconds. Table 3 shows the RMSE of the RMM estimation using the HEKF, allowing for a comparison with the conventional EKF and other existing estimators in the literature. The RMSE corresponding to the optimized HEKF is the lowest compared to the other estimators in each axis. Therefore, the RMM estimation is precise enough regarding the attitude control requirements and the compensation approach may effectively suppress the magnetic disturbance. Figures 4 and 5 illustrate the estimated Euler angles and their corresa ponding estimated error obtained from the HEKF. It can be readily seen that the estimated Euler angles converge accurately to the real ones. Further investigation reveals that the abrupt change in the actual RMM and actuator fault terms also causes slight deterioration of the Euler angles estimation (resulting in a pointing accuracy degradation of approximately 4 degrees) and swiftly regains its good estimation accuracy (with an error of less than 0.1 degree).

Table 3

Comparison of RMM estimation errors

		EKF	HEKF	UKF [27]	EKF [27]
RMSE (Am^2)	M_x	$3.653 \cdot 10^{-4}$	$1.427 \cdot 10^{-4}$	$3.814 \cdot 10^{-4}$	$4.269 \cdot 10^{-4}$
	M_y	$2.359 \cdot 10^{-4}$	$1.736.10^{-4}$	$2.084 \cdot 10^{-4}$	$3.146 \cdot 10^{-4}$
	M_z	$2.795 \cdot 10^{-4}$	$1.111.10^{-4}$	$4.386 \cdot 10^{-4}$	$6.456 \cdot 10^{-4}$
RMSE (deg)	Roll	0.0304	0.0161	—	—
	Pitch	0.0451	0.0297	—	—
	Yaw	0.0820	0.0518	—	—

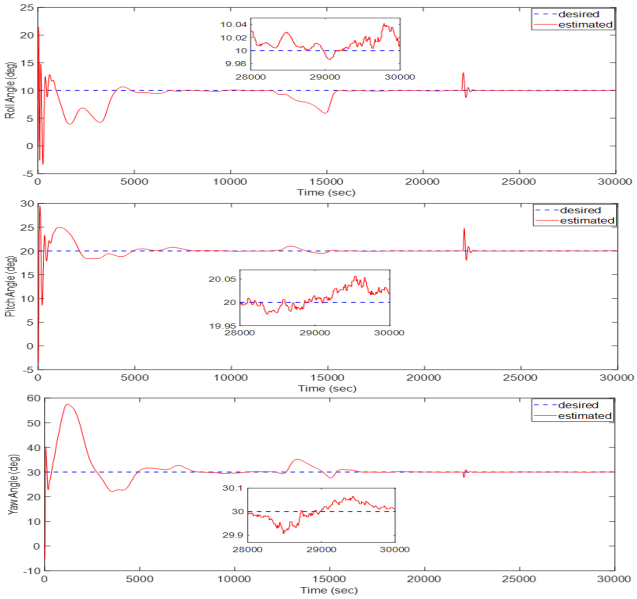

Fig. 4 – Estimated Euler angles for tracking control.

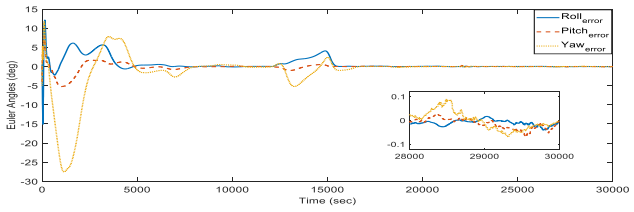

Fig. 5 –Estimated error of the Euler angles.

Furthermore, the actual and predicted torque faults jointly with the actuator fault estimation errors, are presented in Fig. 6. As is obvious, even if all reaction wheels have torque faults, the results prove a good online fault estimation performance throughout the controlling process, where the ac,tuator fault estimation errors remain below $5 \cdot 10^{-6}$ Nm.

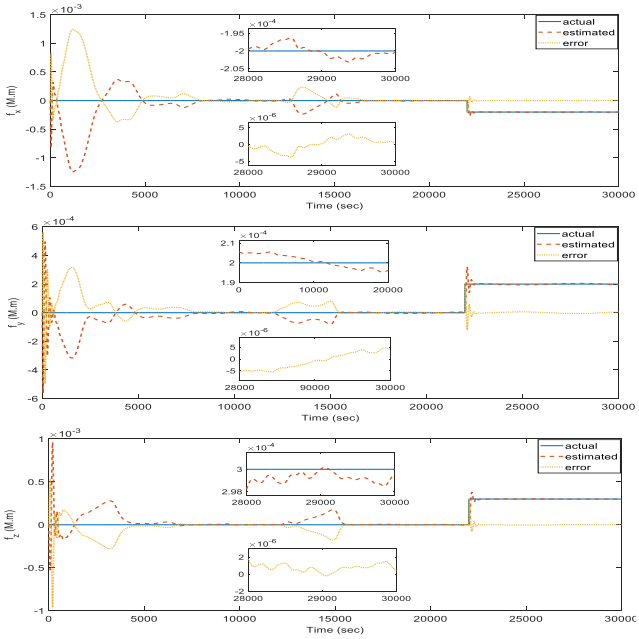

Fig. 6 – Actual and estimated torque fault using APD controller.

6. **CONCLUSION**

In this paper, a new ADCS architecture is proposed, which is based on a HEKF and an adaptive attitude controller. The estimator accurately tracks the attitude of the nanosatellite and agilely captures the actual values of the varying residual RMM. Additionally, the adopted control architecture addresses uncertainties caused by actuator failure and ensures reliable attitude control for nanosatellites. The closed-loop stability of the designed controller is established via Lyapunov analysis. The adopted architecture can effectively mitigate the undesirable impacts caused by RMM and actuator uncertainties, thereby ensuring high precision and reliability in attitude control.

CREDIT AUTHORSHIP CONTRIBUTION STATEMENT

Author_1: Led the conceptualization and methodology development, provided supervision, and contributed to writing and reviewing.
Author_2: Conducted the investigation, performed formal analysis, developed visualizations, and wrote the original draft.
Author_3: Focused on software development and validation.
Author_4: Provided supervision, contributed to writing.

Received on 23 July 2024

REFERENCES

1. Y. Fei, T. Meng, and Z. Jin, *Nano satellite attitude determination with randomly delayed measurements*, Acta Astronautica, **185**, *1*, pp. 319–332 (2021).
2. H. Helvajian, S. Janson, *Small satellites: past, present, and future*, American Institute of Aeronautics and Astronautics, Inc., Aerospace Press, pp. 1–876 (2009).
3. J. E. Benmansour, B. Khouane, *Feed-forward control design for roll/yaw attitude flexible spacecraft based on the disturbance observer*, Rev. Roum. Sci. Techn. – Électrotechn. et Énerg, **67**, *2*, pp. 187–191 (2022).
4. R. Roubache, M. Benyettou, A.M.S Mohammed, A. Boudjemai, A. Bellar, *Impact of the orbital eccentricity on the attitude performance before and after the deorbiting phase for Alsat-1*, Advances in Space Research, **53**, *3*, pp. 474–89 (2014).
5. T. Inamori, N. Sako, S. Nakasuka, *Strategy of magnetometer calibration for nano-satellite missions and in-orbit performance*, In AIAA Guidance, Navigation, and Control Conference, Toronto, Ontario, Canada, pp.7598 (2010).
6. H. E. Soken, S. I. Sakai, *In-orbit estimation of time-varying residual magnetic moment for small satellite applications*, In AIAA Guidance, Navigation, and Control (GNC) Conference, Boston, MA, pp. 4650 (2013).
7. H. E. Soken, S. i. Sakai, *Investigation of estimation methods for time-varying residual magnetic moment*, In H. Haiyan, Procedia Engineering, APISAT, Shanghai, China, pp. 1146–1151 (2015).
8. W. Ley, K. Wittmann, W. Hallmann, *Handbook of space technology*. John Wiley & Sons, Germany, pp. 1–909 (2009).
9. A. Lassakeur, C. Underwood, *Magnetic cleanliness program on cubesats for improved attitude stability*, 9th International Conference on Recent Advances in Space Technologies (RAST), IEEE, Istanbul, Turkey, 11-14 June 2019.
10. R. Srivastava, R. Sah, K. Das, *Attitude and in-orbit residual magnetic moment estimation of small satellites using only magnetometer*, *Small Satellite* Conference, Logan, United States Aug. 7-12, 2021.
11. W. Steyn, Y. Hashida, *In-orbit attitude performance of the 3-axis stabilised SNAP-1 nanosatellite*, *Small Satellite Conference*, Logan, United States, Aug. 13-16, 2001.
12. T. Inamori, N. Sako, S. Nakasuka, *Magnetic dipole moment estimation and compensation for an accurate attitude control in nano-satellite missions*, Acta Astronautica, **68**, *11-12*, pp. 2038–2046 (2011).
13. H. E. Söken, *An attitude filtering and magnetometer calibration approach for nanosatellites,* International Journal of Aeronautical and Space Sciences, **19**, *1*, pp. 164–171 (2018).
14. I. Danil, D. Roldugin, S. Tkachev, M. Ovchinnikov, R. Zharkikh, A. Kudryavtsev, M. Bychek, *Attitude motion and sensor bias estimation onboard the SiriusSat-1 nanosatellite using magnetometer only,* Acta Astronautica, **188**, *1*, pp. 295–307 (2021).
15. L. Li, F. Wang, *An attitude estimation scheme for nanosatellite using micro sensors based on decentralized information fusion*, Optik, **239**, *1*, p. 166886 (2021).
16. K. L. Makovec, A. J. Turner, C. D. Hall, *Design and implementation of a nanosatellite attitude determination and control system*, AAS/AIAA Astrodynamics Specialists Conference, Quebec, Canada, July 30 - August 2, 2001.
17. D. Ran, T. Sheng, L. Cao, X. Chen, Y. Zhao, *Attitude control system design and on-orbit performance analysis of nano-satellite — "Tian Tuo 1"*, Chinese Journal of Aeronautics, **27**, *3*, pp. 593–601 (2014).
18. B. Baghi, M. Kabganian, R. Nadafi, E. Arabi, *Three-axis attitude stabilization of a flexible satellite using non-linear PD controller*, Transactions of the Institute of Measurement and Control, **40**, *2*, pp. 591–605 (2018).
19. A. Adnane, A. Bellar, M. A. S. Mohammed, J. Hong, Z. A. Foitih, *Adaptive Attitude Controller Design for a Rigid Satellite with Feedback Linearization Approach*, The Journal of the Astronautical Sciences, **67**, *4*, pp. 1445–1469 (2020).
20. A. Adnane, H. Jiang, M. A. S. Mohammed, A. Bellar, Z. A. Foitih, *Reliable Kalman filtering for satellite attitude estimation under gyroscope partial failure,* 2nd IEEE Advanced Information Management, Communicates, Electronic and Automation Control Conference (IMCEC), IEEE, Xi'an, China, May 25-27, 2018.
21. S. Zhu, D. Wang, Q. Shen, E. K. Poh, *Satellite attitude stabilization control with actuator faults*, Journal of Guidance, Control, and Dynamics, **40**, *5,* pp. 1304–1313 (2017).
22. C. Stefano, P. Teofilatto, M. S. Farissi, *A magnetometer-only attitude determination strategy for small satellites: Design of the algorithm and hardware-in-the-loop testing*, Aerospace, **7**, *1*, pp. 3 (2020).
23. R. Roubache, M. Benyettou, A. Simohammed, A. Boudjemai, A. Bellar, *Extended Kalman filter for attitude determination of an elliptical orbit satellites,* 6th International Conference on Recent Advances in Space Technologies (RAST), IEEE, Istanbul, Turkey, 12-14 June 2013.
24. F. Hamidia, A. Abbadi, *Improved hybrid pumping system with stockage battery based on particle swarm algorithm*, Rev. Roum. Sci. Techn. – Électrotechn. et Énerg, **66**, *4*, pp. 243–248 (2021).
25. Y. Adel, A. Tlemçani, *An efficient study of PV/wind/battery/electrolyzer/H_2-tank/FC for a remote area electrification*, Rev. Roum. Sci. Techn. – Électrotechn. et Énerg, **69**, *2*, pp. 129–134 (2024).
26. B. Ahcene, A. Oubelaid, A. Chibah, *Comparative study of inner and outer rotor flux reversal permanent magnet machine for direct drive wind turbine*, Rev. Roum. Sci. Techn. – Électrotechn. et Énerg, **69**, *2,* pp. 123–128 (2024).
27. J. Bordeneuve-Guibé, A. Drouin, C. Roos, *Advances in Aerospace Guidance, Navigation and Control*, Springer International Publishing Switzerland, pp. 1–738 (2015).